Membrane Interactions of a Novel Viral Enterotoxin: Rotavirus Nonstructural Glycoprotein NSP4†

Huan Huang,‡ Friedhelm Schroeder,‡ Carl Zeng,§ Mary K. Estes,§ Jonathan K. Schoer,‡ and Judith M. Ball*,‖

Department of Physiology and Pharmacology, Texas A&M University, TVMC, College Station, Texas 77843-4466, Division of Molecular Virology and Microbiology, Baylor College of Medicine, One Baylor Plaza, Houston, Texas 77030, and Department of Pathobiology, Texas A&M University, TVMC, College Station, Texas 77843-4467

Received October 6, 2000; Revised Manuscript Received January 16, 2001

ABSTRACT: The rotavirus enterotoxin, NSP4, is a novel secretory agonist that also plays a role in the unique rotavirus morphogenesis that involves a transient budding of newly made immature viral particles into the endoplasmic reticulum. NSP4 and an active peptide corresponding to NSP4 residues 114 to 135 ($NSP4_{114-135}$) mobilize intracellular calcium and induce secretory chloride currents when added exogenously to intestinal cells or mucosa. Membrane−NSP4 interactions may contribute to these alterations; however, details of a lipid-binding domain are unresolved. Therefore, circular dichroism was used to determine (i) the interaction(s) of NSP4 and $NSP4_{114-135}$ with model membranes, (ii) the conformational changes elicited in NSP4 upon interacting with membranes, (iii) if $NSP4_{114-135}$ is a membrane interacting domain, and (iv) the molar dissociation constant (K_d) of $NSP4_{114-135}$ with defined lipid vesicles. Circular dichroism revealed for the first time that NSP4 and $NSP4_{114-135}$ undergo secondary structural changes upon interaction with membrane vesicles. This interaction was highly dependent on both the membrane surface curvature and the lipid composition. NSP4 and $NSP4_{114-135}$ preferentially interacted with highly curved, small unilamellar vesicle membranes (SUV), but significantly less with low-curvature, large unilamellar vesicle membranes (LUV). Binding to SUV, but not LUV, was greatly enhanced by negatively charged phospholipids. Increasing the SUV cholesterol content, concomitant with the presence of negatively charged phospholipids, further potentiated the interaction of $NSP4_{114-135}$ with the SUV membrane. The K_d of $NSP4_{114-135}$ was determined as well as partitioning of $NSP4_{114-135}$ with SUVs in a filtration-binding assay. These data confirmed NSP4 and its active peptide interact with model membranes that mimic caveolae.

Rotaviruses are the major cause of severe, viral gastroenteritis in young animals and children (*1*). In developing countries, approximately 1 million children die each year from rotavirus infection (*2*−*5*). In the U.S., the annual burden of rotavirus illness in the young is estimated to include over 1 million cases of severe diarrhea and up to 105 deaths (*2*, *5*−*7*).

Rotaviruses undergo a unique morphogenesis in which newly made subviral particles bud into the endoplasmic reticulum (ER) and obtain a transient lipid envelope (*8*−*10*). This process is mediated by the ER-specific, nonstructural viral glycoprotein NSP4 that functions as an intracellular receptor for the subviral particles. As the viral particle matures, the transient membrane is lost by an unknown mechanism, although it has been postulated that NSP4 may play a role in its removal (*11*).

In 1996, a new concept of rotavirus pathogenesis was revealed with the discovery of the first viral enterotoxin, rotavirus NSP4 (*12*). The exogenous addition of NSP4 or the active peptide, $NSP4_{114-135}$, induces an age- and dose-dependent diarrhea in a mouse model and mobilizes intracellular calcium ($[Ca^{2+}]i$) in human intestinal HT29 or *Spodoptera frugiperda* (Sf9) insect cells through phospholipase C (PLC) activation and inositol triphosphate (IP3) production (*12*−*14*). Exogenous addition of NSP4 to isolated colonic crypt cells from both pup and adult mice results in a significant increase in $[Ca^{2+}]i$ (*15*). This non-age-dependent calcium response in isolated crypt cells was surprising and indicates that an event distal to $[Ca^{2+}]i$ mobilization contributes to the age-dependent diarrhea induced by NSP4. Halide permeability was also increased by the exogenous addition of NSP4 to isolated mouse crypt cells that was both

† This work was supported in part by grants from the Texas Advanced Research Program Grant No. 0188-97 (J.M.B.), USPHS National Institutes of Health (GM31651) (F.S.), and DK30144 (M.K.E.).

* To whom correspondence should be addressed: Telephone: 979-845-7910. Fax: 979-845-9231. E-mail: jball@cvm.tamu.edu.

‡ Department of Physiology and Pharmacology, Texas A&M University.

§ Baylor College of Medicine.

‖ Department of Pathobiology, Texas A&M University.

[1] Abbreviations: CD, circular dichroism; DOPS, 1,2-dioleoyl-*sn*-glycero-3-[phospho-L-serine]; Fmoc, fluorenylmethoxycarbonyl; HOAT, 1-hydroxy-7-azabenzotriazole; HPLC, high performance liquid chromatography; IP3, inositol triphosphate; MOPS, 3-[*N*-morpholino]-propanesulfonic acid; NSP4, nonstructural protein 4; PDMS, plasma desorption mass spectrometry; PLC, phospholipase C; PIP2, phosphatidylinositol 4,5-bisphosphate; POPC, 1-palmitoyl-2-oleoyl-*sn*-glycero-3-phosphocholine; Sf9, *Spodoptera frugiperda* insect cells; SUV, small unilamellar vesicles; TDCD, temperature-dependent circular dichroism; TFA, trifluoroacetic acid; TFE, trifluoroethanol.

10.1021/bi002346s CCC: $20.00
Published on Web 03/02/2001

Ca^{2+}- and age-dependent (*15*). These data suggest that NSP4-induced diarrhea is facilitated by a novel membrane permeability pathway (*15*). Given the activity of NSP4, it seems likely that NSP4 interacts with membranes and/or contains a membrane-interactive domain when exogenously added to mammalian cells.

Endogenous expression of NSP4 in Sf9 insect cells also increases cytosolic Ca^{2+}, but the mechanism appears to be distinct from the exogenous addition of NSP4. When NSP4 is expressed in insect cells using a baculovirus expression system, addition of a PLC inhibitor does not affect calcium mobilization (*14*). Despite the importance of these findings, relatively little is known about NSP4−membrane interactions or targeting events associated with the endogenous expression of NSP4 in mammalian cells, nor have structural studies been completed with defined model membranes. Recent data revealed that $NSP4_{112-175}$, a specific cleavage product of NSP4, is released into the media of insect cells when NSP4 is expressed by a baculovirus recombinant (*16*). Thus, endogenously expressed NSP4 may transport from the ER to the plasma membrane in association with lipid vesicles to interact with signaling molecules. Additionally, NSP4 may interact with lipids associated with the plasma membrane as it is released from viral-infected cells.

The present investigation was undertaken to determine if NSP4 and $NSP4_{114-135}$ directly interact with membranes of different curvature and lipid composition. To determine the membrane structural requirements for optimal partitioning with NSP4 and $NSP4_{114-135}$, circular dichroism (CD) was employed. This study shows for the first time the CD structure of purified, full-length NSP4 and the active enterotoxic peptide under physiological conditions. Previous CD spectroscopic analyses of the cytoplasmic tail of NSP4 (residues 86−175) in physiological buffer showed an α-helical content of 22% (*17*). Our new results show that NSP4 and $NSP4_{114-135}$ directly interact with membrane lipids to undergo changes in secondary structure, and these membranes mimic caveolae or caveolae-like microdomains designated as cholesterol-rich rafts (*18*−*20*).

EXPERIMENTAL PROCEDURES

Materials. The phospholipids 1,2-dioleoyl-*sn*-glycero-3-[phospho-L-serine] (DOPS) and 1-palmitoyl-2-oleoyl-*sn*-glycero-3-phosphocholine (POPC) were obtained from Avanti Polar Lipids (Alabaster, AL). Cholesterol, *o*-phthaldialdehyde, trifluoroethanol, and β-mercaptoethanol were purchased from Sigma (St. Louis, MO). Microcon-100 filtration units were obtained from Fisher Scientific Inc. (Pittsburgh, PA). NSP4 protein was isolated as described previously (*21*).

Peptide Synthesis and Characterization. The $NSP4_{114-135}$ peptide (DKLTTREIEQVELLKRIYDKLT) was synthesized by fluorenylmethoxycarbonyl (Fmoc) solid-phase chemistry using an automated Millipore 9050 Plus synthesizer (Perceptive Biosystems Inc., Framingham, MA) and 1-hydroxy-7-azabenzotriazole with di-isopropyl-carbodiimide activation. Addition of 90% trifluoroacetic acid (TFA) in the presence of ethanedithiol (3%), thioanisole (5%), and anisole (2%) resulted in cleavage of the final peptide product from the solid polymer support and removal of side chain protecting groups. After a 2 h incubation, the cleavage mixture was filtered into cold diethyl ether in a polycarbonate tube, the resin was rinsed several times with TFA, and the eluants were combined with the filtrate, dried under N_2, and lyophilized. Unwanted byproducts and organic contaminants were removed from the crude peptide by large scale, gravimetric gel filtration chromatography and monitoring at 215 nm using an ISCO model 229 UV/VIS detector (*22*). This procedure concomitantly partially separates incomplete peptides on the basis of molecular weight. Fractions corresponding to absorbance peaks were pooled separately, lyophilized, and further purified by reverse-phase HPLC using a C4 Delta Pak column (Waters, Milford, MA). Eluted peptide was monitored at 220 nm. Plasma desorption mass spectrometry (PDMS) was used to directly determine the mass of the full-length peptide product and to determine if any other peptide byproduct might be present (Laboratory for Biological Mass Spectrometry, Department of Chemistry, Texas A&M University, College Station, TX). Only those preparations having a correct theoretical mass corresponding to >90% of the total peptide product were used for analysis. $NSP4_{114-135}$ peptide stock solutions were prepared based on the ultraviolet absorption at 280 nm and by amino acid analysis performed at the Protein Chemistry Laboratory, Department of Chemistry, Texas A&M University.

Preparation of Small Unilamellar Vesicles (SUV). SUV composed of POPC/cholesterol (molar ratio 65:35) or POPC/anionic phospholipid (DOPS)/cholesterol (molar ratios 90 to 40:10:0 to 50, respectively) were prepared by sonication using a modification of a method described earlier (*23*, *24*). Stock lipid solutions in $CHCl_3$ were prepared in an amber glass vial. The solvents were removed under N_2 with constant rotation such that the dried lipids formed a thin film on the glass wall and then dried under vacuum a minimum of 4 h. MOPS buffer (10 mM, pH = 7.4, prefiltered through a 0.2 μM filter, Millipore, Bedford, MA) was added, and the sample was vortexed and bath sonicated. The resultant multilamellar membrane suspension was sonicated under N_2 at 4 °C with a microprobe (Sonic Dismembrator model 550, Fisher) at energy level 4 using 1-min pauses after every 2 min sonication to prevent overheating of the lipid solution. The sonicated solution was centrifuged using a 40Ti rotor (Beckman, Fullerton, CA) at a speed of 35K for 4 h to remove any multilamellar vesicles and titanium debris from the sonicator probe. The lipid concentration of the final SUV solution was determined by a standard phosphate assay (*25*).

Preparation of Large Unilamellar Vesicles (LUV). Extrusion through polycarbonate membranes was used to prepare LUV composed of POPC/cholesterol or POPC/cholesterol/DOPS. All procedures were the same as described above for preparation of SUV, except that the sonication step was omitted. Instead, the lipid suspension was extruded 15 times (back and forth) through double layers of 0.1 μm polycarbonate membranes in a mini-extruder (Avanti Polar Lipids, Alabaster, AL).

Photon Correlation Spectroscopy to Determine Size of SUV and LUV. The particle size distribution of SUV and LUV was completed by Beckman-Coulter Inc., Miami, FL, using a Coulter N4 Photon Correlation spectrometer. The particle size range resolved by this instrument was 0.003 to 3 μm diameter.

Membrane Transbilayer Distribution of Phosphatidylserine (DOPS). The membrane transbilayer distribution of DOPS was determined with 2,4,6-trinitrobenzenesulfonic acid

(TNBS), a nonpenetrating chemical probe as described previously (*26*). TNBS reacts with the primary amines of phosphatidylserine or phosphatidylethanol on the outer leaflet of the bilayer yielding the *N*-trinitrophenyl derivative that was monitored by UV spectroscopy (410 nm).

Temperature-Dependent Circular Dichroism (TDCD). The temperature dependence of $NSP4_{114-135}$ and its tendency to aggregate was determined by TDCD. To determine if oligomer formation occurred, TDCD spectra of the $NSP4_{114-135}$ in 10 mM phosphate buffer were obtained using a model 62DF Circular Dichroism spectropolarimeter (Aviv Instruments, Lakewood, NJ) in the laboratory of Dr. Marty Scholtz, Department of Medical Biochemistry and Genetics, Texas A&M University. The signal was monitored at 222 nm. $NSP4_{114-135}$ was prepared at 2, 5, 10, 20, 50, and 100 μM concentrations in phosphate buffer. The temperature was ramped from 0 to 80 °C and then returned to 0 °C in 1° increments. The temperature was equilibrated for 2 min, and the circular dichroic signal was then averaged over 30 s at each temperature.

Circular Dichroism (CD) and Secondary Structure Estimation. The interactions of intact NSP4 and $NSP4_{114-135}$ with SUV and LUV were determined by CD with the following modifications of a previously reported procedure (*27*). Samples contained 4 μM NSP4 or 15 μM $NSP4_{114-135}$ with or without lipid vesicles (1 mM). Samples composed of buffer or lipid vesicles without peptide or protein were used for background correction. CD spectra were obtained at room temperature in a 1-mm circular quartz cell and a model J-710 spectropolarimeter (JASCO Inc, Easton, MD). Each CD spectrum was from 185 to 260 nm with step resolution of 1 nm, speed of 50 nm/min, response of 1 s, bandwidth of 2.0 nm, and sensitivity of 10 mdeg. Data were accumulated from 10 scans, background subtracted, and converted to mean residue molar ellipticity $[\theta]$ (deg cm^2/dmol).

The secondary structure of NSP4 was estimated from the CD data using the program CDsstr developed by W. C. Johnson et al. (*28*, *29*). This method uses a singular value decomposition algorithm as described earlier (*30*). The basis set contains the CD spectra of 22 proteins whose structures are known from high quality X-ray diffraction data. The program randomly chooses the eight proteins for variable selection. Only those combinations where the sum of structures is between 0.952 and 1.05, where no fraction of secondary structure is less than −0.03, and where the reconstructed CD spectrum fits the original CD spectrum with an average root-mean-square error of less than 0.25 units were kept. The protein with unknown structure that was being analyzed was put into the basis set and iterated until the analysis was self-consistent. The results gave estimation of percentage of six protein secondary structure components: α-helix, 3_{10}-helix, β-strand, β-turn, poly(L-proline)II type 3_1-helix, and other.

The equation $\theta_{222} = (f_h - i\kappa/N)[\theta_{h\ 222\infty}]$ was used to determine the percent helix for $NSP4_{114-135}$ (*31*, *32*). In this equation, θ_{222} is the mean residue molar ellipticity at 222 nm, f_h is the fraction in α-helical form, i is the number of helices, κ is a wavelength-specific constant with a value of 2.6 at 222 nm, N is the number of residues in the peptide, and $\theta_{h\ 222\infty}$ is the molar ellipticity for a helix of infinite length at 222 nm (i.e., −39 500 deg cm^2/dmol).

$NSP4_{114-135}$ Partitioning with SUV. In the partitioning experiments, 15 μM of $NSP4_{114-135}$ were incubated with varying total lipid concentrations of SUV or LUV (0 to 4 mM) at 24 °C for a minimum of 10 min. All SUV and LUV had the same lipid composition, i.e., POPC/cholesterol/DOPS = 55/35/10, and were prepared as described above. CD spectra of $NSP4_{114-135}$ were recorded using JASCO J-710 as described above. K_d (reciprocal of the peptide concentration at which 50% of the peptide is partitioned) and binding stoichiometry (n, ratio of DOPS in the outer-leaflet to peptide) were calculated based on a modification of a fluorescence-binding assay (*33*), where $\Delta[\theta]$ and $\Delta[\theta]_{max}$ are measured and applied to the following equation, $1/(1 - \Delta[\theta]/\Delta[\theta]_{max}) = C_L/(\Delta[\theta]/\Delta[\theta]_{max}) \times (1/K_d) - (nE_0)/K_d$. $\Delta[\theta]$ and $\Delta[\theta]_{max}$ indicate the molar ellipticity changes and maximal molar ellipticity changes, respectively, at 222 nm, C_L is the concentration of DOPS in the outer-leaflet of the membrane vesicles, and E_0 is the peptide concentration. The maximum CD changes were obtained from hyperbolar single rectangular fitted curves of $\Delta[\theta]_{222}$ vs the concentration of phosphatidylserine in the outer-leaflet of the membrane vesicles. A plot of $1/(1 - \Delta[\theta]/\Delta[\theta]_{max})$ vs $C_L/(\Delta[\theta]/\Delta[\theta]_{max})$ gave a linear function with a slope of $(1/K_d)$ and an ordinate intercept of $(nE_0)/K_d$ (inset, Figure 6, panel B).

The experiment was repeated in reverse, in that a constant SUV concentration (total lipid concentration of 0.5 mM) was incubated with varying concentrations of $NSP4_{114-135}$ (0 to 40 μM) at 24 °C for a minimum of 10 min. CD spectra of $NSP4_{114-135}$ were recorded using JASCO J-710 as described above. K_d and binding stoichiometry (n) were calculated as above $[1/(1 - \Delta[\theta]/\Delta[\theta]_{max}) = C_L/(\Delta[\theta]/\Delta[\theta]_{max}) \times (1/K_d) - (nE_0)/K_d]$, where $\Delta[\theta]$ and $\Delta[\theta]_{max}$ are measured, C_L is the concentration of $NSP4_{114-135}$, and E_0 is the concentration of DOPS in the SUV outer leaflet. The $\Delta[\theta]_{max}$ were obtained from hyperbolar single rectangular fitted curves of $\Delta[\theta]_{222}$ vs the concentration of $NSP4_{114-135}$. A plot of $1/(1 - \Delta[\theta]/\Delta[\theta]_{max})$ vs $C_L/(\Delta[\theta]/\Delta[\theta]_{max})$ gave a linear function with a slope of $(1/K_d)$ and an ordinate intercept of $(nE_0)/K_d$ (inset, Figure 6, panel C).

Filtration Assay for $NSP4_{114-135}$ Partitioning to Lipid Membranes. The interaction of $NSP4_{114-135}$ ($M_r = 2705$) with membranes was also determined by a filtration assay. A reaction mixture of 12 nmol $NSP4_{114-135}$ and 800 nmol lipid vesicles in a total volume of 200 μL of 10 mM MOPS buffer, pH = 7.4, were incubated at room temperature for 10 min. Each sample was then filtered through a 100 000 molecular weight cutoff filter by centrifugation at 3000 g for 4−7 min through a Microcon-100 filtration unit, until only 5−10 μL remained in the filter unit. Each filter was rinsed with 100 μL of buffer and centrifuged again for 2−3 min. Free peptide in the flow-through fraction was quantified with an *o*-phthaldialdehyde assay and compared to standard curves composed of 1−6 nmol of $NSP4_{114-135}$. In the *o*-phthaldialdehyde assay, 0.5 mL of 0.05 M sodium borate (pH 10) and 0.5 mL of 0.5% (v/v) β-mercaptoethanol in ethanol were added to 100 μL aliquots of $NSP4_{114-135}$. The sample was vortexed well after each addition. A stock solution of *o*-phthaldialdehyde (10 mg/mL in methanol) was diluted 10-fold in 0.05 M borate (pH 10). A 0.5 mL aliquot of this diluted stock solution was added to the above sample while it was vortexed, and the sample was incubated at room temperature for precisely 20 min. Fluorescence intensity

(excitation at 340 nm, emission at 440 nm) was determined with a PC1 Photon Counting fluorescence spectrophotometer (ISS Inc., Champaign, IL). The fluorescence signal is directly proportional to $NSP4_{114-135}$ concentration over the above range.

RESULTS

CD analyses were used to examine whether NSP4 protein and $NSP4_{114-135}$ interact with defined lipid membranes. The effect of membrane curvature on NSP4 and $NSP4_{114-135}$ interaction was resolved using SUV prepared by sonication and LUV prepared by extrusion. To clearly interpret the effect of membrane curvature on the interaction of NSP4 and $NSP4_{114-135}$ with the membranes, it was necessary to characterize the lipid vesicles. In addition, the effects of membrane lipid composition (charge and neutral lipid content) on the membrane curvature and interaction of NSP4 and $NSP4_{114-135}$ with membranes were determined using vesicles containing different percentages of POPC (neutral phospholipid), cholesterol (sterol), and DOPS (anionic phospholipid).

Characterization of the Size Distribution of SUV and LUV Lipid Vesicles. Typically, SUV or LUV diameters are in the range of 25−40 nm or 100−500 nm, respectively (*34*). Given this wide range, it was necessary to determine the size distribution of the SUV and LUV by photon correlation spectroscopy as described in Materials and Methods. SUV, prepared by sonication, had a very narrow size distribution with mean diameters of 20−30 nm and standard deviations of 5−6 nm dependent on lipid composition. The mean diameter of the SUV decreased with increasing amount of negative lipid (DOPS) content, from a mean diameter of 29.2 ± 5.4 nm in the absence of DOPS (POPC/cholesterol/DOPS = 65:35:0), to 24.6 ± 5.6 nm with 10% DOPS (POPC/cholesterol/DOPS = 55:35:10), to 19.5 ± 4.9 nm with 30% DOPS (POPC/cholesterol/DOPS = 35:35:30; $p < 0.05$, Student's t test). However, increasing the cholesterol content from 35 to 50% had no effect on the SUV diameter (24.6 ± 5.6 nm for SUV POPC/cholesterol/DOPS = 55:35:10 vs 26.9 ± 5.6 nm for SUV POPC/cholesterol/DOPS = 40:50:10).

LUV, prepared by extrusion through a stack of two polycarbonate membranes with 100-nm pore size had mean diameters of 100−120 nm with standard deviations of 8−25 nm. When vesicle cholesterol content was kept at 35%, the diameters were 105 ± 25 nm for LUV without DOPS, 118 ± 18 nm for LUV with 10% DOPS, and 112 ± 14 nm for LUV with 30% DOPS. When the vesicle DOPS contents were kept at 10%, the diameters were 118 ± 18 nm for LUV with 35% cholesterol, and 120 ± 8 nm for LUV with 50% cholesterol. In contrast to the results with SUV, the lipid composition had little effect on the mean diameter of the LUV. However, the presence of DOPS and a high level of cholesterol resulted in a more narrow size distribution of the LUV. There was no overlap between the size distributions of SUV and LUV.

Secondary Structure of NSP4 in Aqueous Buffer. To determine if NSP4 protein interactions with membranes alter its secondary structure, the CD spectrum of 1 μM purified NSP4 was first obtained in the absence of membranes in 10 mM aqueous phosphate buffer (pH = 7.4) (Figure 1, dark circles). The CD spectrum showed a double minimum at 208 and 222 nm and a positive peak at 190 nm, consistent with

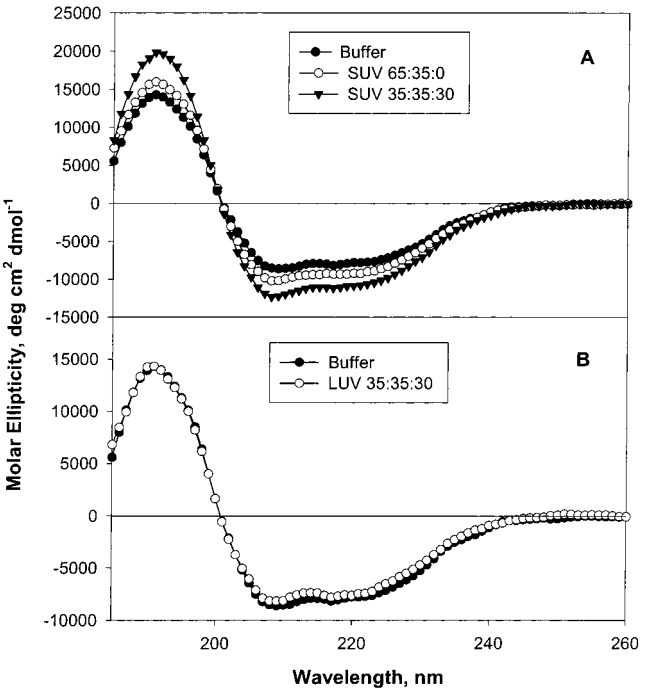

FIGURE 1: Panel A, circular dichroic spectra of NSP4 in the presence of SUV. The symbols refer to NSP4 in the presence of lipid vesicles with the following composition: (●) buffer; (○) POPC/cholesterol/DOPS = 65:35:0; (▼) POPC/cholesterol/DOPS = 35:35:30. Panel B, circular dichroic spectra of NSP4 in the presence of LUV: (●) buffer; (○) POPC/cholesterol/DOPS = 35:35:30. More profound changes are seen in SUVs with increased anionic phospholipid content (panel A, ▼). The NSP4 CD spectrum was not significantly altered in the presence of LUVs with increased DOPS content (panel B, ○).

the presence of α-helical structure in NSP4 (*31*). The percentage of each secondary structure component was estimated using the program CDsstr to be 20% α-helix, 6% 3_{10}-helix, 21% β-strand, 12% β-turn, 7% poly(L-proline) II type 3_1-helix, and 33% other, or more simply, 33% helical structure (Table 1). These data of the entire protein are in agreement with the previously reported 22% α-helical content of NSP4 residues 86−175 (*17*).

NSP4 Interaction with Lipid Vesicles: Effect of Anionic Phospholipid, Membrane Curvature, and Cholesterol. Neither the intracellular distribution of lipids among membrane organelles nor the membrane curvature is uniform. Instead, these parameters vary within any particular membrane depending on the microdomain that is examined (*36*). Consequently, we determined the influence of two of these parameters, charge and radius of curvature, on the interaction(s) of NSP4 with membranes. CD spectra of 1 μM NSP4 in the presence of SUV (Figure 1, panel A) and LUV (Figure 1, panel B) were obtained to examine the effect of curvature; the SUV and LUV contained different percentages of the anionic lipid DOPS to evaluate the effect of charge. The presence of neutral charged SUV vesicles (POPC/cholesterol at molar ratio 65:35) resulted in a small change in the NSP4 CD spectra when compared to aqueous buffer; the molar ellipticity of NSP4 at 222 nm became more negative (−9026 ± 103 vs −7723 ± 96 deg cm^2 dmol^{-1}) (Figure 1, panel A). Concomitantly, the molar ellipticity at 190 nm increased (15974 ± 177 vs 14298 ± 86 deg cm^2 dmol^{-1}). Secondary structure estimations showed a small, but significant increase in the % α-helix (23.8 vs 20%, $p < 0.01$, one way ANOVA)

Table 1: NSP4 Secondary Structure Changes upon Interaction with Lipid Vesicles

	NSP4 secondary structure composition[b]					
type of vesicles[a]	α-helix (%)	3_{10}-helix (%)	β-strand (%)	β-turn (%)	poly(L-proline) II type 3_1-helix (%)	other (%)
buffer	20.0 ± 0	6.3 ± 0.5	21.0 ± 2.0	11.5 ± 1.0	7.0 ± 0.8	33.3 ± 1.7
SUV 65:35:0	23.8 ± 0.5**	6.3 ± 0.5	17.0 ± 0**	11.3 ± 0.5	7.0 ± 0	34.0 ± 0
SUV 35:35:30	30.3 ± 1.0**	7.5 ± 0.6*	12.0 ± 0**	11.5 ± 0.6	6.0 ± 0*	32.0 ± 0
LUV 35:35:30	19.0 ± 0	5.8 ± 0.5	20.8 ± 1.3	11.3 ± 0.5	7.5 ± 0.6	35.0 ± 0.8

[a] Lipid vesicles were prepared as described in the methods section. Lipid compositions are expressed as POPC/cholesterol/DOPS. [b] NSP4 secondary structures were estimated by program CDsstr based on CD spectra as described in the methods section. The results shown are mean ± SD ($n = 4$). *$P < 0.05$, **$P < 0.01$, in an one-way ANOVA test compared to buffer.

and a decrease in β-strand (17 vs 21%, $p < 0.001$, one way ANOVA), while the percentage of other secondary structure components remain unchanged, as compared with that in buffer only (Table 1).

The presence of anionic phospholipid containing SUV (POPC/cholesterol/DOPS at molar ratio 35:35:30) resulted in more profound changes in NSP4 CD spectra as compared to neutral vesicles (Figure 1). With increased anionic phospholipid content in the SUV, the molar ellipticity of NSP4 at 222 nm became more negative (−10662 ± 163 vs. −7723 ± 96 deg cm^2 dmol^{-1}) (Figure 1, panel A), and the molar ellipticity at 190 nm increased (19865 ± 209 vs 14298 ± 86 deg cm^2 dmol^{-1}) as compared to buffer only or neutral vesicles. These spectral changes, consistent with increased α-helical content were quantitatively analyzed as described in Materials and Methods. Based on these calculations, the NSP4 α-helix increased from 20 to 30.3% ($p < 0.01$, one way ANOVA) and β-strand content decreased from 21 to 12% ($p < 0.01$, one way ANOVA) in the presence of SUV containing 30% DOPS (Table 1).

In the presence of anionic phospholipid containing LUV (POPC/cholesterol/DOPS at molar ratio 35:35:30), the CD spectrum and calculated secondary structure of NSP4 was basically the same as in aqueous buffer suggesting that the radius of curvature is important to NSP4 membrane interactions (Figure 1, panel B, and Table 1). There was no statistical difference in the structure of NSP4 in buffer and in the presence of LUV ($p > 0.05$, one way, ANOVA, Table 1). Taken together, these data clearly show that NSP4 preferentially interacts with lipid vesicles containing anionic phospholipid and having a high radius of curvature. However, the bulk of the NSP4 structure may not necessarily interact with the membrane to undergo changes in secondary structure to reflect increased α-helical content, but rather a specific region. This issue was further addressed through use of the active $NSP4_{114-135}$ peptide (see below).

Distribution of Phosphatidylserine (DOPS) in the Outer Leaflet of SUV and LUV Membranes. The preferential interaction of NSP4 with SUV as compared to LUV was not dependent on the absolute composition of the lipids. However, the molecular basis for the preferential interaction with anionic SUV could be due to differences in the distribution of lipids within the leaflets of the SUV and LUV membranes. This possibility was examined by measuring the transbilayer distribution of the anionic phosphatidylserine in SUV and LUV with the nonpenetrating chemical probe TNBS. As shown in Table 2, 10.9 ± 0.4% of the outer leaflet phospholipid in SUV containing 10% DOPS (55:35:10) was phosphatidylserine. Increasing the SUV total DOPS to 30% only increased the percentage of the outer leaflet DOPS to 16.4 ± 0.3%. In contrast, 61.9 ± 1.0% of the inner leaflet phospholipid in SUV containing 30% DOPS (55:35:30) was phosphatidylserine (Table 2). Increased cholesterol in the SUV did not affect the percentage of the outer leaflet DOPS. In summary, DOPS was preferentially localized to the inner leaflet of the SUV at high, but not low, mol % DOPS.

Table 2: Phosphatidylserine (DOPS) Distribution in Lipid Vesicles

	% phosphatidylserine[b]			
	SUV[c]		LUV[d]	
vesicle lipid composition[a]	outer leaflet	inner leaflet	outer leaflet	inner leaflet
55:35:10	10.9 ± 0.4	7.8 ± 1.1	7.3 ± 0.2	12.7 ± 0.5
40:50:10	11.3 ± 0.4	7.1 ± 1.2	6.7 ± 0.4	13.3 ± 0.5
35:35:30	16.4 ± 0.3	61.9 ± 1.0	11.5 ± 0.5	48.6 ± 0.7

[a] Vesicle lipid composition was expressed as mole ratio of POPC/cholesterol:DOPS. [b] Negatively charged phospholipid (DOPS) distribution was determined by TNBS assay as described in Materials and Methods. The results were calculated as percentage of PS out of total phospholipid in each leaflet, based on the total phospholipid distribution of outer leaflet/inner leaflet = 70:30 for SUVs and 50:50 for LUVs (*26*, *69*). The results are presented as mean ± SD, $n = 3$. [c] SUVs were prepared by probe sonication as described in Materials and Methods. [d] LUVs were prepared by extrusion through a stack of two polycarbonate membranes with pore size 0.1 μm as described in Materials and Methods.

The DOPS distribution in each leaflet of LUV differed from those of the SUV. Regardless of lipid composition, the percentage of the outer leaflet phospholipid represented by DOPS was always significantly lower ($p < 0.001$, Student's t test) in LUV than the corresponding SUV (Table 2). However, increasing the mol % of DOPS in the LUV membranes to 30 mol % total DOPS resulted in 11.5% of the outer leaflet phospholipid as DOPS, similar to that of SUV containing only 10 mol % total DOPS. Also similar to SUV, there was a significant increase in DOPS in the inner leaflet of LUV membranes prepared with 30% DOPS.

Temperature-Dependent Circular Dichroism (TDCD) of $NSP4_{114-135}$. The peptide segment comprising amino acids 114−135 of the NSP4 protein has enterotoxic activity and has been postulated to represent a membrane interaction domain. Further, an elongated, cytoplasmic region of NSP4 that includes residues 114−135 was shown to fold as a coiled-coil (*17*). Therefore, $NSP4_{114-135}$ was synthesized and evaluated similarly as the NSP4 protein. Prior to testing its interaction with membranes, it was important to optimize the concentration-dependent properties of the peptide to preclude peptide aggregation that could confound interpretation of CD data. This was particularly important with the $NSP4_{114-135}$ peptide since analysis of its amino acid sequence predicted a high amphipathic score (AS = 35) suggesting

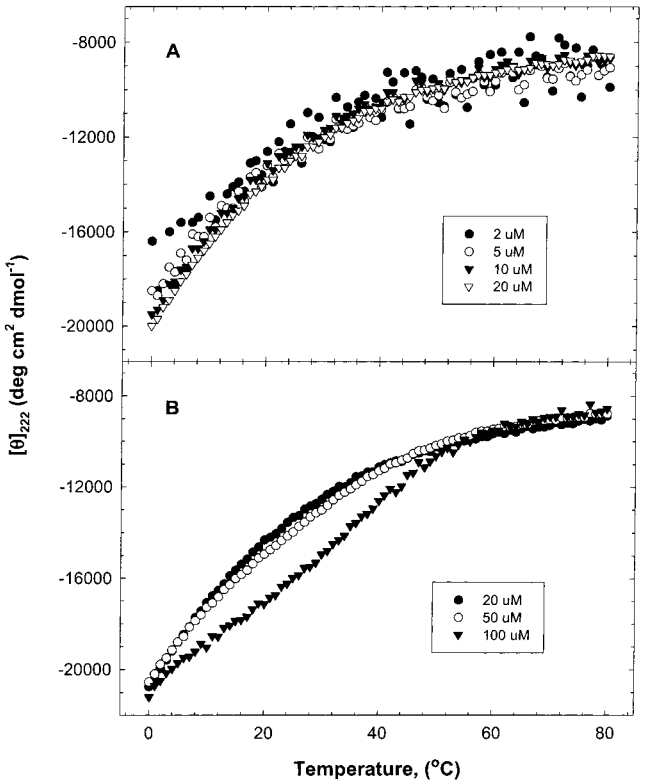

FIGURE 2: Temperature-dependent molar ellipticity at 222 nm of various concentrations of $NSP4_{114-135}$ in 10 mM phosphate buffer. Panel A shows that at concentrations between 2 and 20 μM the 114−135 peptide does not aggregate. Panel B shows that at peptide concentrations $\geq$50 μM, the peptide aggregates or forms oligomers. The symbols and associated values in each panel refer to the concentration of $NSP4_{114-135}$ peptide.

that dimers or higher order oligomers or aggregates of the peptide may form at elevated concentrations (*35*). Such aggregates of $NSP4_{114-135}$ could themselves undergo CD shifts as compared to the soluble form, thereby seriously complicating determination of the interaction of this peptide with membranes by CD. Therefore, the optimal $NSP4_{114-135}$ concentration at which oligomers or aggregates were absent was determined by monitoring the CD signal at 222 nm as a function of peptide concentration in phosphate buffer solution. At concentrations between 2 and 20 μM $NSP4_{114-135}$, the CD signal was independent of concentration at all temperatures between 0 and 80 °C (Figure 2, panel A). This is consistent with the absence of $NSP4_{114-135}$ aggregation over this concentration range. There was a small deviation in the CD signal at a concentration of 50 μM $NSP4_{114-135}$ (Figure 2, panel B) and a much higher deviation at 100 μM $NSP4_{114-135}$, indicating the formation of oligomers or aggregation of the peptide. Therefore, all subsequent CD experiments were performed at $NSP4_{114-135}$ peptide concentrations $<$20 μM.

Finally, the observation of a decrease in $NSP4_{114-135}$ signal intensity with increasing temperature at peptide concentrations between 2 and 20 μM was consistent with progressive unfolding of the $NSP4_{114-135}$ α-helical structure with increased temperature. At approximately 60 °C, the structure was fully disordered (Figure 2, panel B). The curves shown in Figure 2 were reversible upon cooling (data not shown), indicating that the unfolding of the peptide was also reversible.

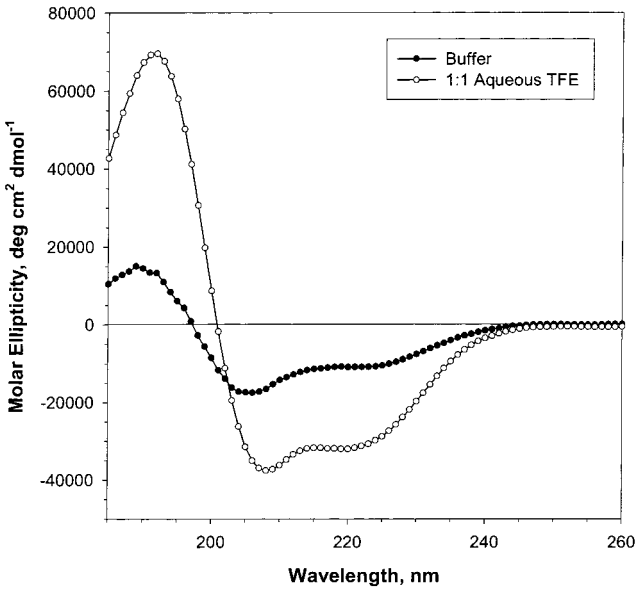

FIGURE 3: Circular dichroic spectra of $NSP4_{114-135}$ in aqueous buffer only (●) or 1:1 aqueous trifluoroethanol (○). The aqueous trifluoroethanol enhanced the hydrophobic environment and the propensity of the 114−135 peptide to fold in a helical structure.

Secondary Structure of $NSP4_{114-135}$ in Aqueous Buffer. The secondary structure of $NSP4_{114-135}$ in aqueous buffer was revealed by CD spectra (Figure 3, filled circles). The appearance of double minima at 208 and 222 nm and a positive peak at 190 nm indicates that the $NSP4_{114-135}$ peptide adopted a secondary structure with a high α-helical content. Calculations based on the molar ellipticity at 222 nm showed that $NSP4_{114-135}$ adopted a secondary structure that contained 37% α-helix in buffer (*31*).

Trifluoroethanol (TFE) favors secondary structure in peptides and proteins by promoting intramolecular hydrogen bonding. Therefore, the propensity for $NSP4_{114-135}$ to form helical structure in a more hydrophobic environment was determined by measuring CD spectra in aqueous solution containing TFE. The CD spectra of $NSP4_{114-135}$ in TFE/aqueous (1:1) differed markedly from those in aqueous buffer. The spectrum of the peptide in TFE/aqueous (1:1) indicates a significant increase in α-helical structure, with an even more negative molar ellipticity at 208 and 222 nm, and more positive molar ellipticity at 190 nm (Figure 3, open circles). The isodichroic point at about 205 nm suggests that the structural transformation was from random coil to α-helix. The α-helical content for $NSP4_{114-135}$ in TFE/aqueous (1:1) was estimated at 91% from the molar ellipticity at 222 nm.

In summary, $NSP4_{114-135}$ spontaneously adopted some α-helical structure in aqueous buffer. The formation of a α-helical structure was dramatically enhanced in a more hydrophobic solvent environment suggesting that the interaction of $NSP4_{114-135}$ with membranes (more hydrophobic environment in the bilayer interior) might elicit similar changes. This possibility was examined in experiments described in the following section.

Effect(s) of Anionic Phospholipids on Membrane Interaction with $NSP4_{114-135}$. The effect(s) of increasing the anionic phospholipid (DOPS) content of the SUV and LUV membranes on the interaction with $NSP4_{114-135}$ peptide was examined (Figure 4). In the presence of neutral vesicles

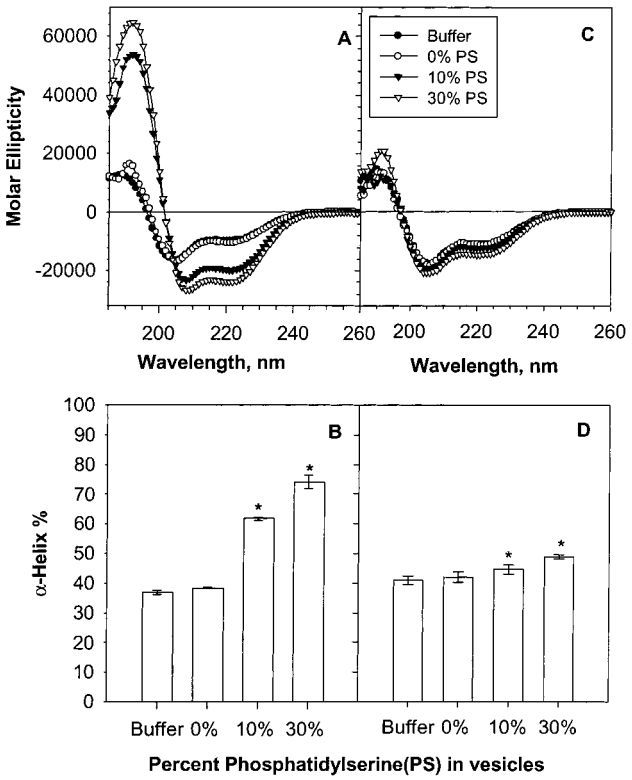

FIGURE 4: Circular dichroic spectra of $NSP4_{114-135}$ in the presence of SUV (panel A) or LUV (panel C) with increasing anionic phospholipid content. Panels A and C: $NSP4_{114-135}$ in the presence of buffer only (●); SUV or LUV, POPC/cholesterol/DOPS = 65:35:0 (○); SUV or LUV, POPC/cholesterol/DOPS = 55:35:10 (▼); SUV or LUV, POPC/cholesterol/DOPS = 35:35:30 (▽). The % α-helical content of $NSP4_{114-135}$ in the presence of SUV (panel B) or LUV (panel D) with increasing anionic phospholipid content is shown with the *y* axis indicating the % α-helix and the *x* axis indicating the % phosphatidylserine (DOPS) in the liposome preparation. Data represent the mean ± SD. *, $p < 0.001$, one way ANOVA, as compared to buffer alone.

composed of POPC/cholesterol (molar ratio 65:35), the CD spectrum and calculated α-helical content of the 114−135 peptide were not significantly altered as compared to that in buffer alone regardless of the vesicle size ($p > 0.05$, one way ANOVA) (Figure 4, panels A and B, SUV; panels C and D, LUV). In contrast, in the presence of SUV containing anionic phospholipid (POPC/cholesterol/DOPS, 55/35/10 and 35/35/30), the CD spectra of $NSP4_{114-135}$ were increasingly and significantly changed (Figure 4, panel A, solid triangles and open triangles vs solid circles). In the presence of anionic SUVs, the CD spectra of $NSP4_{114-135}$ showed more α-helical characteristics, i.e., more negative molar ellipticity at 222 and 208 nm, and more positive molar ellipticity at 190 nm. The isodichroic point at about 205 nm suggested that the structural transformation was from random coil to α-helix. Calculations based on molar ellipticity at 222 nm showed a significant increase in α-helix ($p < 0.01$, one way ANOVA), in the presence of SUV containing 10% DOPS (62% α-helix) and 30% DOPS (76% α-helix) (Figure 4, panel B). Thus, the presence of anionic phospholipids in SUV membranes reacted with peptide more than doubled the α-helical content of $NSP4_{114-135}$.

In the presence of anionic LUV, the CD spectrum of $NSP4_{114-135}$ only changed slightly with a small increase in α-helical structure with increasing anionic phospholipid content in the LUV (Figure 4, panel C). Calculations based on molar ellipticity at 222 nm showed a small, but significant increase in α-helical content in the presence of negative LUV ($p < 0.01$, one way ANOVA). However, these changes were much smaller when compared to increasing the negative charge of the SUV with the same lipid composition ($p < 0.0001$, unpaired t test).

These results indicate that $NSP4_{114-135}$ preferentially interacts with negatively charged vesicles to adopt a more α-helical conformation. This interaction was strongest with membranes containing increasing mol % of anionic phospholipid and high membrane surface curvature. The maximal increases in α-helical content of the $NSP4_{114-135}$ peptide (more than 2-fold) were much greater than those observed with the complete NSP4 protein (Figure 1). This observation was consistent with $NSP4_{114-135}$ representing a specific membrane-binding domain in the NSP4 polypeptide chain.

Effect(s) of SUV Cholesterol Content on Membrane Interaction with $NSP4_{114-135}$. Although the anionic phospholipid content of most membranes is maintained in a fairly narrow range, the cholesterol content of intracellular membranes varies widely. Cholesterol content ranges from >50 mol % in cholesterol-rich membranes (e.g., plasma membranes) to 4−10 mol % in cholesterol poor membranes (e.g., retinal rod outer segment and inner mitochondrial membranes) (*36*−*39*). Plasma membrane microdomains such as caveolae and caveolae-like lipid rafts have 3−4-fold as much cholesterol as the surrounding plasma membrane (*40*). The above studies showed that $NSP4_{114-135}$ interacted most strongly with POPC/cholesterol SUV containing anionic phospholipid. We therefore examined the effect of cholesterol content on the interaction of $NSP4_{114-135}$ with highly curved, anionic SUV.

The effect of increasing cholesterol content from 0 to 50 mol % on the CD spectra of $NSP4_{114-135}$ interacting with negative SUV (DOPS maintained constant at 10 mol %) is shown in Figure 5, panel A. In the absence of cholesterol, i.e., POPC/DOPS at a molar ratio of 90:10, the anionic SUV interacted significantly less with the peptide ($p < 0.01$, one way ANOVA). With increasing amounts of cholesterol in the anionic SUV, the peptide became substantially more α-helical upon membrane interaction as indicated by the molar ellipticity at 222 nm becoming more negative and molar ellipticity at 190 nm becoming more positive ($p < 0.01$, one way ANOVA). The isodichroic point at 205 nm suggested that the $NSP4_{114-135}$ structure changed from random coil to α-helix. At the highest cholesterol content tested (50 mol %), the % α-helix of $NSP4_{114-135}$ increased nearly 2-fold as compared to the peptide in aqueous buffer and 1.4-fold as compared to the peptide interacting with anionic SUV with 0% cholesterol (Figure 5, panel B). As indicated in the preceding section, the presence of cholesterol alone was insufficient for peptide interaction with the SUV in that there were no CD spectral changes upon interaction with neutral SUV containing POPC/cholesterol (65/35). Thus, both cholesterol and anionic phospholipids were necessary for optimal interaction with the $NSP4_{114-135}$ peptide.

In the presence of LUV lacking cholesterol, there were no significant changes in peptide secondary structure when compared to buffer alone ($p > 0.05$, one way ANOVA) (Figure 5, panels C and D). When the LUV cholesterol

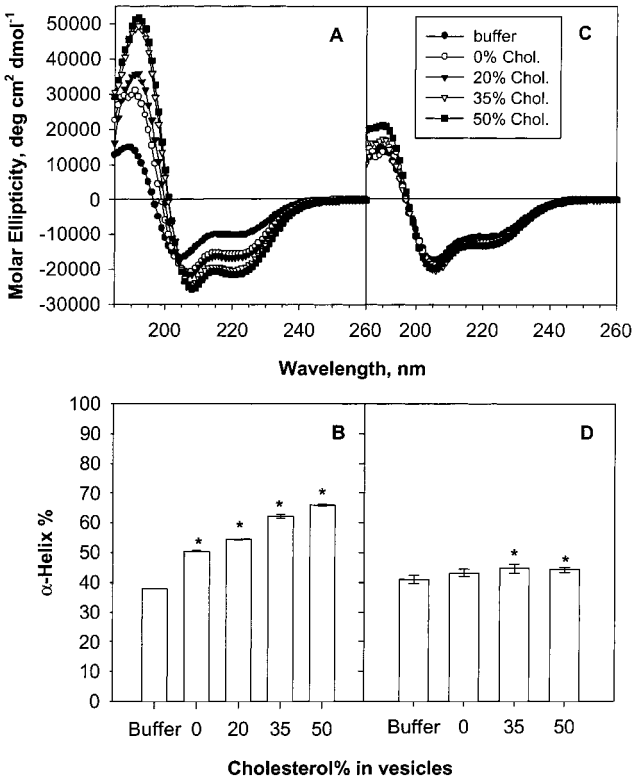

FIGURE 5: Circular dichroic spectra of $NSP4_{114-135}$ in the presence of SUV (panel A) or LUV (panel C) with increasing cholesterol content. Panel A, $NSP4_{114-135}$ in the presence of buffer only (●); SUV or LUV, POPC/cholesterol/DOPS = 90:0:10 (○); SUV or LUV, POPC/cholesterol/DOPS = 70:20:10 (▼); SUV or LUV, POPC/cholesterol/DOPS = 55:35:10 (▽); SUV, POPC/cholesterol/DOPS = 40:50:10 (■). The % α-helical content of $NSP4_{114-135}$ in the presence of SUV (panel B) or LUV (panel D) with increasing cholesterol content is shown with the *y*-axis indicating the % α-helix and the *x* axis indicating the % cholesterol in the liposome preparation. Data represent the mean ± SD. *, $p < 0.001$, unpaired t test, compared to buffer alone.

content was increased to 35 or 50%, there was a small, but significant increase in peptide helical structure when compared to buffer alone ($p < 0.01$, one way ANOVA). Still, $NSP4_{114-135}$ secondary structure alterations in the presence of SUV with the same cholesterol content as the LUV, was significantly higher ($p < 0.01$, one way ANOVA) (Figure 5).

In summary, $NSP4_{114-135}$ preferentially adopted a more α-helical conformation upon interaction with negatively charged SUV membranes containing high mol % cholesterol. The presence of cholesterol alone was insufficient to induce an interaction of the peptide with SUV. Both cholesterol and anionic phospholipid were necessary for optimal interaction with $NSP4_{114-135}$. The interactions were stronger with increasing amount of cholesterol present in the anionic SUV.

Partitioning of $NSP4_{114-135}$ with SUV and LUV: CD Analyses. The relative affinity of $NSP4_{114-135}$ for SUV vs LUV with the same lipid composition, POPC/cholesterol/DOPS = 55:35:10, at varying concentrations was examined by CD measurements at 222 nm. The CD signal of $NSP4_{114-135}$ at 222 nm became more negative and finally close to saturation as the peptide associated with an increasing concentration of SUV (Figure 6, panel A). Upon partitioning to LUV with the same lipid composition and different concentrations, very little CD changes were observed.

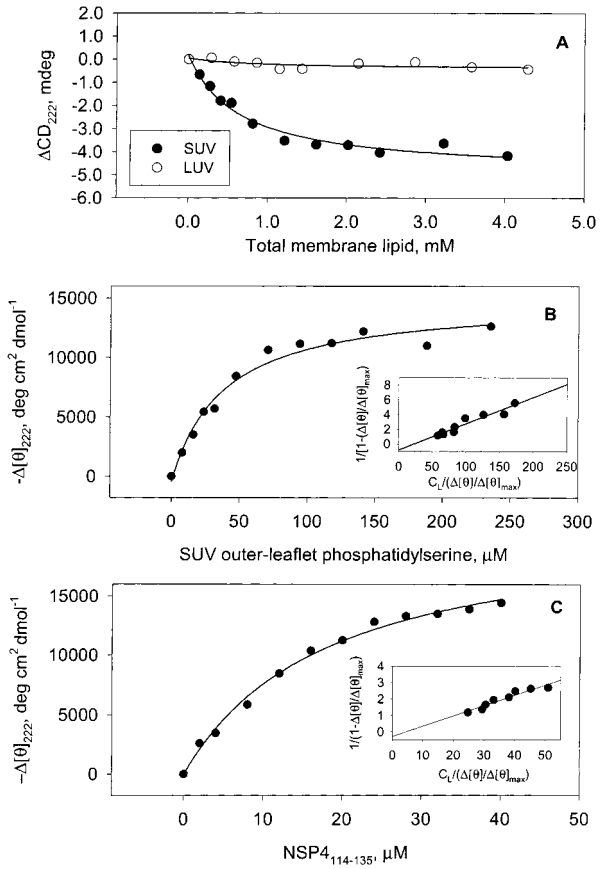

FIGURE 6: Association of $NSP4_{114-135}$ with model membranes. Panel A, representative partitioning curve of $NSP4_{114-135}$ with SUV (black circles) and LUV (open circles). SUV and LUV have the same lipid composition, POPC/cholesterol/DOPS = 55/35/10. Partitioning experiments were carried out at 24 °C, pH = 7.4, with peptide $NSP4_{114-135}$ concentration 15 μM. The solid lines are hyperbolic single rectangular fitted curves. Panel B, representative saturation curve of peptide $NSP4_{114-135}$ (15 μM) molar ellipticity changes at 222 nm vs concentration of phosphatidylserine in the SUV outer-leaflet. Inset, linear least-squares plot of $1/(1 - \Delta[\theta]/\Delta[\theta]_{max})$ vs $C_L/(\Delta[\theta]/\Delta[\theta]_{max})$ for $NSP4_{114-135}$ with SUV. Panel C, representative saturation curve of peptide $NSP4_{114-135}$ molar ellipticity changes at 222 nm vs concentration of peptide while the SUV concentrations were kept constant at 0.5 mM. Inset, linear least-squares plot of $1/(1 - \Delta[\theta]/\Delta[\theta]_{max})$ vs $C_L/(\Delta[\theta]/\Delta[\theta]_{max})$.

The dissociation constant (K_d) and binding stoichiometry (n) for $NSP4_{114-135}$ partitioning to SUV were calculated as follows. The data $\Delta[\theta]_{222}$ vs the concentration of DOPS in the outer-leaflet of the membrane vesicles were fitted with hyperbolar single rectangular curve (Figure 6, panel B) from which the maximum CD changes were obtained. The plot $1/(1 - \Delta[\theta]/\Delta[\theta]_{max})$ vs $C_L/(\Delta[\theta]/\Delta[\theta]_{max})$ gave a linear function, ($r^2 \sim 0.9$) (Figure 6, panel B, inset). K_d and n, calculated from the slope of $(1/K_d)$ and ordinate intercept of $(nE_0)/K_d$, were 25.6 ± 1.5 μM, and 1.87 ± 0.15, respectively (mean ± SE, $N = 4$). The value n is the partitioning ratio of DOPS in the outer-leaflet to peptide.

In the reverse binding experiment, the concentration of SUV was kept constant at 0.5 mM total lipid and the peptide concentration was increased from 0 to 40 μM. K_d and n were calculated as above. Briefly, the experimental data $\Delta[\theta]_{222}$ vs the concentration of $NSP4_{114-135}$ were fitted with hyperbolar single rectangular curve (Figure 6, panel C), the

maximum CD changes were noted, and a linear function, ($r^2 \sim 0.95$) (Figure 6, panel C, inset) was derived from a plot of $1/(1 - \Delta[\theta]/\Delta[\theta]_{max})$ vs $C_L/(\Delta[\theta]/\Delta[\theta]_{max})$. K_d and n calculated from the slope ($1/K_d$) and ordinate intercept ($nE_0)/K_d$ were 15.1 ± 2.5 μM, and 0.17 ± 0.02, respectively (mean $\pm$ SE, $N = 4$) where n is the partitioning ratio of peptide to DOPS in the outer leaflet.

Comparison of the two binding curves (Figure 6, panels B and C) reveals the maximum molar ellipticity changes were lower when the concentration of the peptide was held constant (Figure 6, panel B) than when the SUV concentration was held constant. Moreover, the ratio of DOPS in the outer-leaflet to peptide was lower when the peptide concentration was held constant and the lipid concentration varied ($1/n = 1.87$) when compared to holding the lipid concentration constant and varying the concentration of $NSP4_{114-135}$ ($n = 5.9$). There are several possible explanations for the observed differences in K_d and n based on the two assays in which the concentration of lipid vs peptide varied. As the SUV concentration increases, there is an accompanying increase in light scatter which in turn lowers the CD signal and causes the partitioning curve to prematurely reach its maximum (*41*). Another explanation is the difference in lipid accessibility in the two assays, i.e., as the SUV concentration increases, the availability of both sides of the vesicle for peptide partitioning decreases (*42*).

The above observations in the partitioning assay are consistent and corroborate the data from the CD experiments in which there was little or no CD changes of the peptide in the presence of neutral lipid vesicles or LUV. The partitioning assay also confirmed that $NSP4_{114-135}$ interacts more favorably with lipid vesicles that are highly curved, rich in anionic phospholipid, and enriched in cholesterol.

$NSP4_{114-135}$ Partitioning to SUV and LUV: A Filtration Assay. In the presence of neutral SUV and all LUVs, CD spectra of $NSP4_{114-135}$ showed little or no increase in α-helical content. These data can be explained in two ways, first, less peptide partitioned to the lipid vesicles; second, upon partitioning, $NSP4_{114-135}$ underwent less secondary structural changes. To resolve these possibilities, the extent of $NSP4_{114-135}$ partitioning to SUV and LUV was determined by an independent direct filtration assay. The $NSP4_{114-135}$ peptide was incubated with SUV or LUV, and the free peptide was separated from the partitioned peptide by filtration through a 100 000 molecular cutoff filter. The free $NSP4_{114-135}$ in the flow-through portion was then determined by reaction with *o*-phthaldialdehyde. In this binding experiment, the concentration of different membrane vesicles and the concentration of the peptide were kept the same for all the samples. Furthermore, the peptide-to-lipid ratio were kept the same as those in the CD experiments. The results are presented as percent free peptide (mean $\pm$ SD, $n = 4$) (Figure 7).

There was basically no partitioning of $NSP4_{114-135}$ to neutral membrane vesicles regardless of the vesicle size, since approximately 100% of the peptides were in the flow-through fraction. When the percent of negative phospholipid (DOPS) in SUV increased, a greater percentage of peptide was partitioned to the SUVs. The percent of free peptide dropped to 92% when the percent DOPS in SUV increased to 10%. The percent of free peptide dropped to only 19% when the SUV contained 30% DOPS. When the percentage of cholesterol in SUV was increased (DOPS % kept at 10%), an increase in partitioning of the peptide to the SUV was observed (Figure 7).

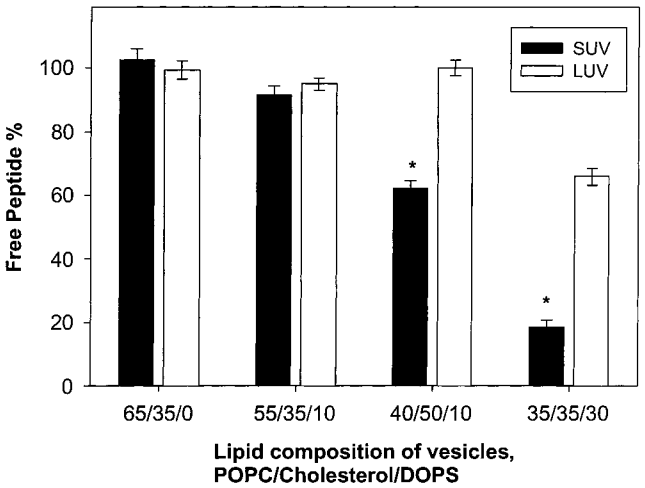

FIGURE 7: Partitioning of $NSP4_{114-135}$ to lipid vesicles. Partitioning of $NSP4_{114-135}$ to SUV and LUV was determined by a filtration assay as described in Materials and Methods. Data are presented as mean $\pm$ SD, $n = 4$. *, significant difference between partitioning to SUV and LUV, $p < 0.001$, one way ANOVA.

As compared to the partitioning to SUV with the same lipid composition, $NSP4_{114-135}$ showed much lower affinity to LUVs. The peptide only showed significant partitioning (66% free peptide) to LUV containing 30% DOPS; however, the partitioning was much weaker than that with SUV with the same lipid composition. In all other cases, no significant partitioning was observed between $NSP4_{114-135}$ and the LUVs (Figure 7).

The above observations in the filtration assay are consistent with the CD experiments, indicating that the little or no CD changes of the peptide in the presence of neutral lipid vesicles and LUVs are due to little or no partioning to the membrane vesicles. The filtration assay also confirmed that $NSP4_{114-135}$ preferentially interacts with lipid vesicles that are highly curved, rich in anionic phospholipid, and highly enriched in cholesterol.

DISCUSSION

The data presented herein provide several important new insights regarding the interaction of the first described viral enterotoxin, NSP4 and its active peptide $NSP4_{114-135}$, with membranes. Purified NSP4 and $NSP4_{114-135}$ both undergo secondary structure alterations (i.e., increased α-helix formation) upon interaction with specific types of model membranes. These conformational changes may be important for the biological activity of NSP4, especially in eliciting signal transduction pathways via lipid secondary messenger molecules (*13*, *14*, *43*). NSP4 and the 114−135 peptide interacted with vesicles composed exclusively of lipids indicating other types of molecules (e.g., glycoproteins or glycolipids) were not necessary for the structural alterations or binding. Thus, NSP4 and $NSP4_{114-135}$ are membrane-active. This membrane interaction was evident from a significant change in NSP4 secondary structure, i.e., increase in α-helical content upon SUV membrane interaction rich in anionic phospholipid and partitioning of $NSP4_{114-135}$ in a binding filtration assay. However, it must be recognized that the actual magnitude

of the change in NSP4 protein secondary structure upon interaction with membranes rich in anionic phospholipid may be obscured, at least in part, by the presence of an extended polypeptide chain structure composed of additional helical regions that are not part of a membrane interaction domain.

NSP4 and $NSP4_{114-135}$ preferentially interacted with a membrane lipid domain that is highly curved, rich in anionic phospholipid, and highly enriched in cholesterol. This lipid microdomain could in itself be construed as a type of "receptor" defined by a specific structure and lipid composition. The bulk of the NSP4 structure may not necessarily interact with the membrane to undergo changes in secondary structure to reflect increased α-helical content, but rather a specific region could represent a lipid "binding domain". Similar "receptors" for bacterial cytolysins have been reported to be cholesterol-rich membrane microdomains in both model membranes (*44*, *45*) and biological membranes (*44*, *46*, *47*). Interestingly, limited proteolysis of these cytolysins eliminates the cytolytic, but not the cholesterol binding activity of these cytolysins (*46*, *47*). It remains unknown if proteolysis of NSP4 would eliminate the membrane interaction or enterotoxic activity.

$NSP4_{114-135}$ is 100-fold less active than the native protein in inducing diarrhea indicating that the segment encompassing amino acids 114−135 does not represent the complete enterotoxic domain or fails to fold in the correct conformation for full activity (*12*). However, the 114−135 peptide maintains full binding activity of the membrane vesicles. Perhaps the 114−135 region of NSP4 is a membrane-binding domain that "stabilizes" the interaction of NSP4 with its receptor when NSP4 is added to the outside of cells. Whereas, in endogenously expressed NSP4, residues 114−135 may stabilize the interaction of NSP4 with phosphatidylinositol 4,5-bisphosphate (PIP2) or direct NSP4 to specific lipid domains containing other mediators of signal transduction in the plasma membrane.

The interaction of NSP4 and $NSP4_{114-135}$ with membranes was dependent on the vesicles having a high radius of curvature. As the diameter of the membrane vesicle decreases, the radius of curvature increases (*34*). The high curvature of SUV results in more mobile packing of the phospholipid headgroups in the outer leaflet and an increased packing constraint in the inner leaflet (*48*). The net result is a highly exposed hydrophobic core that likely facilitates the interaction of SUV with protein hydrophobic domains (*49*). The radius of curvature of the SUV is so small that the molar ratio of total lipid in the outer monolayer to total lipid in the inner monolayer can be as large as 2:1. Thus, the ratio of the inner-to-outer monolayer lipids is indicative of the radius of curvature and illustrates the packing restrictions of lipids in small radius of curvature bilayers. For example, SUV with a diameter of 25 nm has an outer membrane to inner membrane lipid ratio of 2.2:1 (mole ratio) (*34*). In contrast, the mean diameter of the LUV is larger, and the distribution of lipid between the outer and inner monolayers is close to 1:1. The molar ratio of lipid in the outer and inner leaflets in LUV with a mean diameter of 100 is 1.2:1 (*34*). Thus, the membranes of SUV (mean diameters of 20−30 nm) have a significantly higher curvature, i.e., a more restricted packing, and an inner-to-outer lipid ratio of ∼2:1 when compared to the membranes of LUV (mean diameters of 100−120 nm) wherein the inner-to-outer lipid ratio is ∼1:1.

Other membrane binding proteins, such as Factor Va light chain, mellitin, and the somastatin analogue, also show substantial preference for binding SUV over LUV (*48*, *50*−*53*). Most cell membranes are heterogeneous with defined regions of high curvature. Highly curved membrane regions are prevalent in the intestinal microvillus (*54*, *55*), the site of NSP4 protein enterotoxic activity. Other membrane regions with a high radius of curvature include caveolae, found in both the plasma membrane and associated with the endoplasmic reticulum and golgi (reviewed in ref *40*); clathrin coated pits in the plasma membrane (reviewed in ref *56*); and shed membrane vesicles (*57*). The structural basis of NSP4 and $NSP4_{114-135}$ interaction with highly curved membranes likely includes the more mobile packing and lower surface pressure of the phospholipids in the outer leaflet of SUV and the hydrophobic, restricted domain of the inner leaflet (*53*, *58*, *59*).

The inclusion of negatively charged phospholipids also influenced the interaction of NSP4 and $NSP4_{114-135}$ with SUV, although the interaction was not solely due to the degree of exposed anionic phospholipid in the outer leaflet. Increasing the content of anionic phospholipid in the outer leaflet of LUV to the same extent as in SUV did not reverse the lack of interaction. The functional significance of these findings with model membranes to biological membranes is the presence of plasma membrane microdomains rich in anionic phospholipid. For example, plasma membrane caveolae are membrane microdomains rich in anionic phospholipid as well as cholesterol (*20*, *60*, *61*, reviewed in ref *40*). Although caveolae constitute about 1% of the plasma membrane surface area, about 10% of the plasma membrane cholesterol are contained in caveolae (*41*). The binding activity of NSP4 was potentiated in the presence of anionic phospholipid and cholesterol. Further, the K_d data showed $NSP4_{114-135}$ have specific membrane structural (i.e., high curvature) as well as lipid compositional requirements for optimal membrane partitioning.

The K_d obtained in this study is in the range of K_d values previously reported with peptide and model membranes (*41*, *42*, *62*). For example, different regions of the 79-residue apolipoprotein C-II (apoC-II) bind to lipid surfaces with a K_d of 0.4−6.0 μM (*41*). The $apoC\text{-}II_{19-39}$ peptide is a random coil in aqueous solution, converts to 60% α-helix when mixed with SUV, and binds with a K_d of 6.0 μM (*63*). Other reported K_d values of peptide−membrane interactions were considerably higher, i.e., in the mM range (*64*). A difference in $NSP4_{114-135}$ K_d values were noted when the partitioning assay was reversed such that the SUV concentrations were increased and the peptide concentration was maintained. A similar difference in K_d was reported when the association of an amphipathic, helical peptide to model membranes was determined by changing either the peptide or lipid vesicle concentration (*42*). In this report, the K_d value was 2-fold less when the peptide concentration was maintained and the model membrane concentration varied than when the lipid vesicle concentration was maintained and the peptide concentration varied (*42*).

All of the characteristics of the model membranes necessary for optimal interaction with NSP4 and $NSP4_{114-135}$ (high membrane curvature, rich in cholesterol and anionic phos-

pholipids) are also characteristic of caveolae membrane domains. This connection may be physiologically significant in view of compartmentalization of signaling molecules in caveolae, such as those involved in NSP4 function, including PIP2, Ca^{2+} ATPase, calmodulin, IP3 receptors, and G proteins (*60*, *65*, *66*). As much as 50% of cellular PIP2 compartmentalizes in caveolae and IP3 is generated in caveolae (*67*−*71*). Therefore, endogenously expressed NSP4 may transport to and interact with caveolae membranes and exogenously added NSP4 may be targeted to G proteins localized to caveolae. Additional experiments are needed to confirm this hypothesis.

REFERENCES

1. Kapikian, A. Z., and Chanock, R. M. (1996) in *Virology* (Fields, B. N., Knipe, D. M., and Howley, P. M., Eds.) Lippincott-Raven Press, Philadelphia, PA.
2. Bern, C., and Glass, R. I. (1994) in *Viral Infections of the Gastrointestinal Tract* (Kapikian, A. Z., Ed.) Marcel Dekker, Inc., New York.
3. Kapikian, A. Z., and Chanock, R. M. (1989) in *Viral Infections of Humans* (A. S., Evans, Ed.) Plenum Press, New York.
4. World Health Organization (1973) *WHO Weekly Epidemiol. Rec. 48*, 409−416.
5. Walsh, H. A., and Warren, K. S. (1979) *N. Engl. J. Med. 301*, 967−974.
6. Guerrant, R. L., Hughes, J. M., Lima, N. L., and Crane, J. (1990) *Rev. Inf. Dis. 12*, S41−S50.
7. Ho, M.-S., Glass, R. I., Pinsky, P. F., and Anderson, L. L. (1988) *J. Infect. Dis. 158*, 1112−1116.
8. Au, K. S., Chan, W. K., Burns, J. W., and Estes, M. K. (1989) *J. Virol. 63*, 4553−4562.
9. Au, K. S., Mattion, N. M., and Estes, M. K. (1993) *Virology 194*, 665−673.
10. Meyer, J. C., Bergmann, C. C., and Bellamy, A. R. (1989) *Virology 171*, 98−107.
11. Tian, P., Ball, J. M., Zeng, C., and Estes, M. K. (1996) *J. Virol. 70*, 6973−6981.
12. Ball, J. M., Tian, P., Zeng, C. Q. Z., Morris, A. P., and Estes, M. K. (1996) *Science 272*, 101−104.
13. Dong, Y., Zeng, C. Q. Z., Ball, J. M., Estes, M. K., and Morris, A. P. (1997) *Proc. Natl. Acad. Sci. U.S.A. 94*, 3960−3965.
14. Tian, P., Hu, Y., Schilling, W. P., Lindsay, D. A., Eiden, J., and Estes, M. K. (1994) *J. Virol. 68*, 251−257.
15. Morris, A. P., Scott, A. K., Zeng, C. Q. Z., Ball, J. M., and O'Neal, W. K. (1999) *Am. J. Phys. 277*, G431−G444.
16. Zhang, M. L., Zeng, C. Q.-Y., Morris, A. P., and Estes, M. K. (2000) *J. Virol. 74* 11663−11675.
17. Taylor, J. A., O'Brien, J. A., and Yeager, M. (1996) *EMBO J. 15*, 4469−4476.
18. Brown, D. A., and London, E. (1998) *Annu. Rev. Cell Dev. Biol. 14*, 111−136.
19. Parton, R. G. (1996) *Curr. Opin. Cell Biol. 8*, 542−548.
20. Anderson, R. (1998) *Annu. Rev. Biochem. 67*, 199−225.
21. Tian, P., Ball, J. M., Zeng, C. Q. Z., and Estes, M. K. (1996) *J. Virol. 70*, 6973−6981.
22. Fontenot, J. D., Ball, J. A., Miller, M. A., David, C. M., and Montelaro, R. C. (1991) *Pept. Res. 4*, 19−25.
23. Schroeder, F., Barenholz, Y., Gratton, E., and Thompson, T. E. (1987) *Biochemistry 26*, 2441−2448.
24. Hapala, I., Kavecansky, J., Butko, P., Scallen, T. J., Joiner, C., and Schroeder, F. (1994) *Biochemistry 33*, 7682−7690.
25. Ames, B. N. (1968) *Methods Enzymol. 8*, 115−118.
26. Litman, B. J. (1973) *Biochemistry 12*, 2545−2554.
27. Stolowich, N. J., Frolov, A., Atshaves, B. P., Murphy, E., Jolly, C. A., Billheimer, J. T., Scott, A. I., and Schroeder, F. (1997) *Biochemistry 36*, 1719−1729.
28. Johnson, W. C. (1999) *Proteins: Struct. Funct., Genet. 35*, 307−312.
29. King, S. M., and Johnson, W. C. (1999) *Proteins: Struct., Funct., Genet. 35*, 313−320.
30. Compton, L. A., and Johnson, W. C., Jr. (1986) *Anal. Biochem. 155*, 155−167.
31. Chen, Y.-H., Yang, J. T., and Chau, K. H. (1974) *Biochemistry 13*, 3350−3359.
32. Keler, T., and Sorof, S. (1993) *J. Cell Physiol. 157*, 33−40.
33. Frolov, A., Cho, T. H., Billheimer, J. T., and Schroeder, F. (1996) *J. Biol. Chem. 271*, 31878−31884.
34. Cullis, P. R., Fenske, D. B., and Hope, M. J. (1996) in *Biochemistry of Lipids, Lipoproteins and Membranes* (Vance, D. E., and Vance, J. E., Eds.) Elsevier Sciences B. V., The Netherlands.
35. Margolit, H., Spouge, J. L., Cornette, J. L., Cease, K. B., Delisi, C., and Berzofsky, J. A. (1987) *J. Immunol. 138*, 2213−2229.
36. Schroeder, F., Frolov, A. A., Murphy, E. J., Atshaves, B. P., Jefferson, J. R., Pu, L., Wood, W. G., Foxworth, W. B., and Kier, A. B. (1996) *Proc. Soc. Exp. Biol. Med. 213*, 150−177.
37. Schroeder, F., Frolov, A., Schoer, J., Gallegos, A., Atshaves, B. P., Stolowich, N. J., Scott, A. I., and Kier, A. B. (1998) in *Intracellular Cholesterol Trafficking* (Chang, T. Y., and Freeman, D. A., Eds.) Kluwer Academic Publishers, Boston, MA.
38. Liscum, L., and Dahl, N. K. (1992) *J. Lipid Res. 33*, 1239−1254.
39. Rose, T. M., Schultz, E. R., Sasaki, G. C., Kolattukudy, P. E., and Shoyab, M. (1994) *DNA Cell Biol. 13*, 669−678.
40. Smart, E. J., and van der Westhuyzen, D. R. (1998) in *Intracellular Cholesterol Trafficking* (Chang, T. Y., and Freeman, D. A., Eds.) Kluwer Academic Publishers, Boston, MA.
41. MacPhee, C. E., Howlett, G. J., and Sawyer, W. H. (1999) *Anal. Biochem. 275*, 22−29.
42. Polozov, I. V., Polozova, A. I., Mishra, V. K., Anantharamaiah, G. M., Segrest, J. P., and Epand, R. M. (1998) *Biochim. Biophys. Acta 1368*, 343−354.
43. Tian, P., Estes, M. K., Hu, Y. Z., Ball, J. M., Zeng, C. Q. Z., and Schilling, W. P. (1995) *J. Virol. 69*, 5763−5772.
44. Ohno-Iwashita, Y., Iwamoto, M., Mitsui, K., Ando, S., and Iwashita, S. (1991) *J. Biochem. 110*, 369−375.
45. Ohno-Iwashita, Y., Iwamoto, M., Ando, S., and Iwashita, S. (1991) *Biochim. Biophys. Acta 1109*, 81−90.
46. Ohno-Iwashita, Y., Iwamoto, M., Mitsui, K., Ando, S., and Nagai, Y. (1988) *Eur. J. Biochem. 176*, 95−101.
47. Ohno-Iwashita, Y., Iwamoto, M., Ando, S., Mitsui, K., and Iwashita, S. (1990) *Biochim. Biophys. Acta 1023*, 441−448.
48. Vaccaro, A. M., Tatti, M., Ciaffoni, F., Salvioli, R., Barca, A., and Roncaioli, P. (1993) *Biochim. Biophys. Acta 1149*, 55−62.
49. Vaccaro, A. M., Tatti, M., Ciaffoni, F., Salvioli, R., Barca, A., and Roncaioli, P. (1993) *Biochim. Biophys. Acta 1149*, 2213−2229.
50. Abbott, A. J., and Nelsestuen, G. L. (1987) *Biochemistry 26*, 7994−8003.
51. Greenhut, S. F., Bourgeois, V. R., and Roseman, M. A. (1986) *J. Biol. Chem. 261*, 3670−3675.
52. Wischut, J. C., Regts, J., Westenberg, H., and Scherpof, G. (1978) *Biochim. Biophys. Acta 508*, 185−196.
53. Machida, K., and Ohnishi, S. I. (1980) *Biochim. Biophys. Acta 596*, 201−209.
54. Lipka, G., Schulthess, G., Thurnhofer, H., Wacker, H., Wehrli, E., Zeman, K., Weber, F. E., and Hauser, H. (1995) *J. Biol. Chem. 270*, 5917−5925.
55. Boffelli, D., Weber, F. E., Compassi, S., Werder, M., Schulthess, G., and Hauser, H. (1997) *Biochemistry 36*, 10784−10792.
56. Fielding, C. J., and Fielding, P. E. (1997) *J. Lipid Res. 38*, 1503−1521.
57. Kavecansky, J., Schroeder, F., and Joiner, C. H. (1995) *Am. J. Physiol. 269*, C1105−C1111.
58. Talbot, W. A., Zheng, L. X., and Lentz, B. R. (1997) *Biochemistry 36*, 5827−5836.
59. Subirade, M., Salesse, C., Marion, D., and Pezolet, M. (1995) *Biophys. J. 69*, 974−988.
60. Parton, R. G. (1996) *Curr. Opin. Cell Biol. 8*, 542−548.

61. Anderson, R. G. W. (1993) *Proc. Natl. Acad. Sci. U.S.A. 90*, 10909−10913.
62. van't Hof, R., and de Kruijff, B. (1995) *FEBS 361*, 35−40.
63. MacPhee, C. E., Howlett, G. J., Sawyer, W. H., and Clayton, H. A. (1999) *Biochemistry 38*, 10878−10884.
64. Chen, Y., Ludescher, R. D., and Montville, T. J. (1998) *App. Environ. Microbiol. 64*, 3530−3532.
65. Fujimoto, T. (1993) *J. Cell Biol. 120*, 1147−1157.
66. Shaul, P. W., and Anderson, R. G. W. (1998) *Am. J. Phys. 275*, L843−L851.
67. Pike, L. J., and Casey, L. (1996) *J. Biol. Chem. 271*, 26453−26456.
68. Fujimoto, T., Nakade, S., Miyawaki, A., Mikoshiba, K., and Ogawa, K. (1992) *J. Cell Biol. 119*, 1507−1513.
69. Hope, H. R., and Pike, L. J. (1996) *Mol. Biol. Cell 7*, 843−851.
70. Li, S., Okamoto, T., Chun, M., Sargiacomo, M., Casanova, J. E., Hansen, S. H. N. I., and Lisanti, M. P. (1995) *J. Biol. Chem. 270*, 15693−15701.
71. Schnitzer, J. E., Oh, P., Jacobson, B. S., and Dvorak, A. M. (1995) *Proc. Natl. Acad. Sci. U.S.A. 92*, 1759−1763.

BI002346S